Journal of Power Sources 210 (2012) 163–171

Contents lists available at SciVerse ScienceDirect

Journal of Power Sources

journal homepage: www.elsevier.com/locate/jpowsour

Influence of ytterbium on the electrochemical property of PbCaSn alloy in sulfuric acid solution

D.G. Li*, J.D. Wang, D.R. Chen

State Key Laboratory of Tribology, Tsinghua University, Beijing 100084, China

ARTICLE INFO

Article history:
Received 4 February 2012
Received in revised form 8 March 2012
Accepted 12 March 2012
Available online 21 March 2012

Keywords:
Electrochemical property
Ytterbium
Lead–calcium-tin alloy
Anodic film
Lead acid battery

ABSTRACT

The influence of ytterbium on the electrochemical property of PbCaSn alloy in 4.5 mol L^{-1} H_2SO_4 solution is studied by cyclic voltammetry (CV), linear sweep voltammetry (LSV), electrochemical impedance spectroscopy (EIS) and Mott–Schottky plot. The results show that Yb can improve the corrosion resistance of PbCaSn alloy in 4.5 mol L^{-1} H_2SO_4 solution. Mott–Schottky plot reveals that the anodic film on PbCaSn alloy at 1.28 V_{SCE} appears an n-type semi-conductive character, Yb can decrease the slope of M–S plot, implying the increment of the defect density within the anodic film, which is beneficial to improve the conductivity of the anodic film. According to the results obtained from EIS, it can be found that the growth of Pb(II) compounds ($PbSO_4$·PbO, $3PbSO_4$·PbO and PbO) is significantly inhibited by adding Yb.

1. Introduction

Generally, PbCa alloy is widely used as the grid material for the maintenance-free lead acid battery [1,2], owing to its high over-potential of hydrogen evolution. The over-potential of hydrogen evolution on PbCa alloy is higher than that on PbSb alloy, which is resulting in the low water consumption and the small self-discharge, and then PbCa alloy can be suitable for the grid material of the maintenance-free applications or valve regulated lead acid battery (VRLA). However, PbCa alloy has an unfavorable factor usually referred to the premature capacity loss (PCL), which is attributed to a high impedance barrier layer formed on the grid surface. Previous papers report that the barrier layer is mainly composed of PbO, which has quite high resistivity (about 10^{11} Ω cm^2), such high resistance can significantly impede the electronic conduction between the grid surface and the active material, and then the capacity of lead acid battery decreases sharply, this is the so-called "premature capacity loss (PCL)" [3–6].

In order to improve the film conductivity and the charge–discharge performance of lead acid battery, Sn is added into PbCa alloy. According to Giess [7], Sn suppresses the transformation of lead to alpha PbO, and inhibits the growth of Pb(II) compound in the anodic film. However, the "PCL" cannot be thoroughly eliminated by the addition of Sn, and excessive Sn content may increase the self-discharge of lead acid battery [8,9]. A lot of new grid materials have been studied in recent years to resolve the PCL [10,11], but the results are still unsatisfied. Adding alloy element into PbCaSn alloy is obviously an effective method to solve "PCL" problem, in our previous work, it has been found that adding the rare-earth element, such as Ce, into PbCaSn alloy can increase the conductivity of the anodic film [12]. Ytterbium is another rare-earth element, how does it affect the electrochemical property of PbCaSn alloy in sulfuric acid solution? Fewer papers focus on this issue. In this paper the novel alloy (PbCaSnYb) is manufactured by adding Yb into PbCaSn alloy, the influence of Yb on electrochemical behaviors of PbCaSn electrode in 4.5 mol L^{-1} H_2SO_4 is investigated using linear sweep voltammetry (LSV), cyclic voltammetry (CV), electrochemical impedance spectroscopy (EIS) and Mott–Schottky plot.

2. Experimental

2.1. Material and sample

The experimental material is prepared by weighed mixture of pure lead (99.99 wt%), pure tin (99.99 wt%), pure calcium (99.99 wt%) and pure ytterbium (99.99 wt%) in an electric furnace with nitrogen as protect gas. Ca, Sn, Yb and Al are added into lead molten at 1000 K, the addition of a little amount of Al can prevent the loss of Ca and Yb, after adequate stirring for 10 min. When the molten temperature drops to 723 K, the molten alloy is poured into a copper mould in the atmosphere to form the blank rod (Φ20 mm × 200 mm), and the rod samples are machined in a form of wafer (Φ10 mm × 5 mm). The compositions of the casting alloys

* Corresponding author. Tel.: +86 10 6279 5148; fax: +86 10 6278 1379.
E-mail address: dgli@mail.tsinghua.edu.cn (D.G. Li).

0378-7753/$ – see front matter © 2012 Elsevier B.V. All rights reserved.
doi:10.1016/j.jpowsour.2012.03.037

Table 1
Chemical composition of the cast alloys.

Alloy	Mass content fraction (wt%)				
	Ca	Sn	Yb	Al	Sn/Ca
PbCaSn	0.042	1.35	0	0.0013	32.14
PbCaSnYb-1	0.043	1.34	0.023	0.0011	31.16
PbCaSnYb-2	0.045	1.33	0.048	0.0012	29.56
PbCaSnYb-3	0.044	1.36	0.086	0.0011	30.9

are determined by chemical analysis, the result is listed in Table 1. One end surface of the sample exposed in the electrolyte acted as the working surface is abraded with 2000 grit SiC paper, polished with 0.5 μm Al_2O_3 powder and then cleaned using double-distilled water, while other surfaces are sealed with epoxy resin in the lower part of an L-shaped glass tube. The anodic films are formed at 1.28 V (vs. SCE) in 4.5 mol L^{-1} H_2SO_4 for EIS, Mott–Schottky plot and LSV experiments.

2.2. Electrochemical experiments

All electrochemical experiments are performed in a conventional three-electrode cell, the counter and reference electrodes are a platinum mesh and SCE, respectively. All potentials mentioned in this paper are referred as the reference electrode.

The cyclic voltammetry is carried out at CH Instrument model 750 electrochemical working station. The potential scanning range is from 1 V to 2 V with a 5 mV s^{-1} scanning rate.

The linear sweep voltammetry (LSV) is performed at EG&G instrument model 273A electrochemical working station. The working electrode is polarized at −1.2 V for 20 min to remove the oxidation film formed on the electrode surface. Then, the anodic film is formed at 1.28 V for 12 h in 4.5 mol L^{-1} H_2SO_4 solution. After the film formation, the working electrode is immediately scanned from 1.28 V to −1 V with a scanning rate of 2 mV s^{-1}.

Mott–Schottky plot of the anodic film at 1.28 V is also carried out at EG&G instrument model 273A electrochemical working station with a 10 mV s^{-1} scanning rate, the scanning potential range is from 0 V to 2 V, and the measured frequency is 1000 Hz.

EIS apparatus is consisted of EG&G instrument model 273A electrochemical working station with 5210 frequency response analyzer, the potential is increased by 10 mV and the sweeping frequency is from 100 kHz to 5 mHz.

3. Results and analysis

3.1. Cyclic voltammetry (CV)

The corrosion behaviors of PbCaSnYb alloy in 4.5 mol L^{-1} H_2SO_4 solution can be depicted by cyclic voltammetries. Fig. 1 shows the cyclic voltammetries of four electrodes for 100 cycles at different temperatures. It can be seen that the cyclic voltammetries of four electrodes display similar features, three peaks donated as m, n and o can be observed in the positive scanning process, beginning at ca. 1.4 V, 1.85 V, and 2.0 V, respectively. Furthermore, a large cathodic peak p is formed at about 1.38 V. In which peak m is associated with the oxidation of the inner PbO, $PbSO_4$ and matrix lead into α-PbO_2, peak n is related to the formation of β-PbO_2 from $PbSO_4$, and peak o corresponding to the oxygen evolution. In the cathodic scanning, peak p represents the reduction of α-PbO_2 into $PbSO_4$ [13]. The current densities of peaks m, n and p decrease with the increment of Yb content in PbCaSn alloy at one fixed temperature in case of every electrode, indicating the increased corrosion resistance of PbCaSn alloy in 4.5 mol L^{-1} H_2SO_4 solution, similar result is obtained by Liu on PbCaSn alloy [14]. While the oxygen evolution curve during charging begins at a lower voltage when the amount of ytterbium

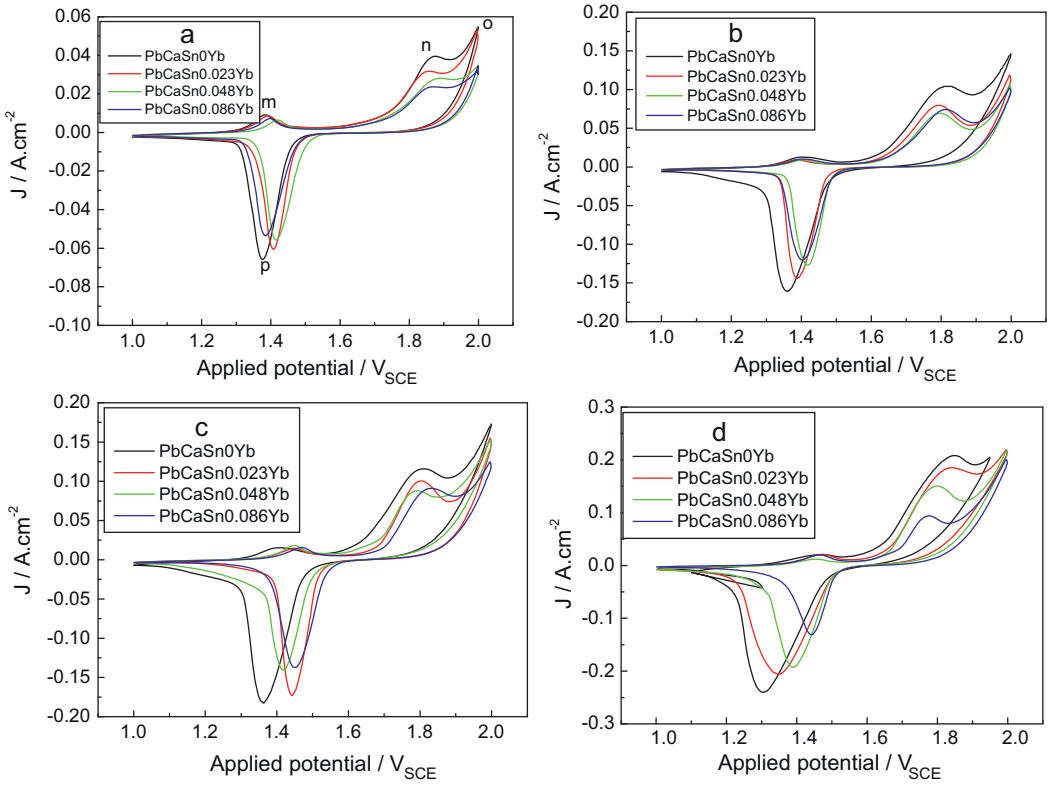

Fig. 1. Cyclic voltammetries after 100 cycles of Pb0.035%Ca1.2%Sn, Pb0.035%Ca1.2%Sn0.023%Yb, Pb0.035%Ca1.2%Sn0.048%Yb and Pb0.035%Ca1.2%Sn0.086%Yb electrodes in 4.5 mol L^{-1} H_2SO_4 solution under different temperatures: (a) 25 °C, (b) 45 °C, (c) 60 °C and (d) 75 °C.

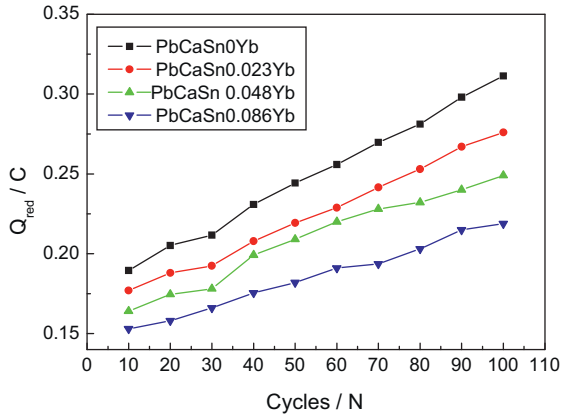

Fig. 2. Variation of the reduction charges of peak d for PbCaSn alloy with different Yb contents and the cycles.

increases, this may cause higher rates of gas evolution and faster dry-out of the battery, and it indicates that the addition of Yb may improve the oxygen evolution of PbCaSn alloy in sulfuric acid solution. Additionally, the peak currents increase with the increment of the cycle for every electrode, the reason can be related to the increased corrosion of the electrode and the increasing specific surface area of the corrosion film with cycle.

Fig. 2 shows the variation of the reduction charge (corresponding to peak d) in the cyclic voltammetries of four electrodes and the cycles, it can be seen that there is a good linear relationship between the reduction charges (Q_{red}) and the cycles (N) in case of every electrode. The slope of the Q_{red}–N plot in the case of Pb0.035%Ca1.2%Sn electrode is 0.00135 C N^{-1}, 0.00113 C N^{-1} for Pb0.035%Ca1.2%Sn0.023%Yb electrode, 0.0009643 C N^{-1} for Pb0.035%Ca1.2%Sn0.048%Yb electrode and 0.0007512 C N^{-1} for Pb0.035%Ca1.2%Sn0.086%Yb electrode, respectively. Significantly, the increase rate of the reduction charges (the fitted slope) of PbCaSn alloy decreases with the increment of Yb content, hence, it can be concluded that the addition of Yb may improve the corrosion resistance of PbCaSn alloy in 4.5 mol L^{-1} H_2SO_4 solution.

In order to specify the influence of Yb on the corrosion behavior of PbCaSn alloy in H_2SO_4 solution, the SEM images of corrosion scales after cyclic voltammetries for 100th on four electrodes in 4.5 mol L^{-1} solution at 25 °C are shown in Fig. 3. Apparently, the features of the corrosion particles on four electrodes are different, the corrosion scale on PbCaSn alloy appears amorphous, the corrosion scales become more crystalline and the corrosion particle grows with the increment of Yb, the porosity of the corrosion scale sharply decreases with the increment of Yb content.

3.2. Polarization curve of PbCaSnYb alloy

The potentiodynamic curves of Pb0.035%Ca1.2%Sn, Pb0.035%Ca1.2%Sn0.023%Yb, Pb0.035%Ca1.2%Sn0.048%Yb and Pb0.035%Ca1.2%Sn0.086%Yb electrodes in 4.5 mol L^{-1} solution at 25 °C are shown in Fig. 4, it can be seen that PbCaSnYb electrode is in the passive state in the large potential region, the passive

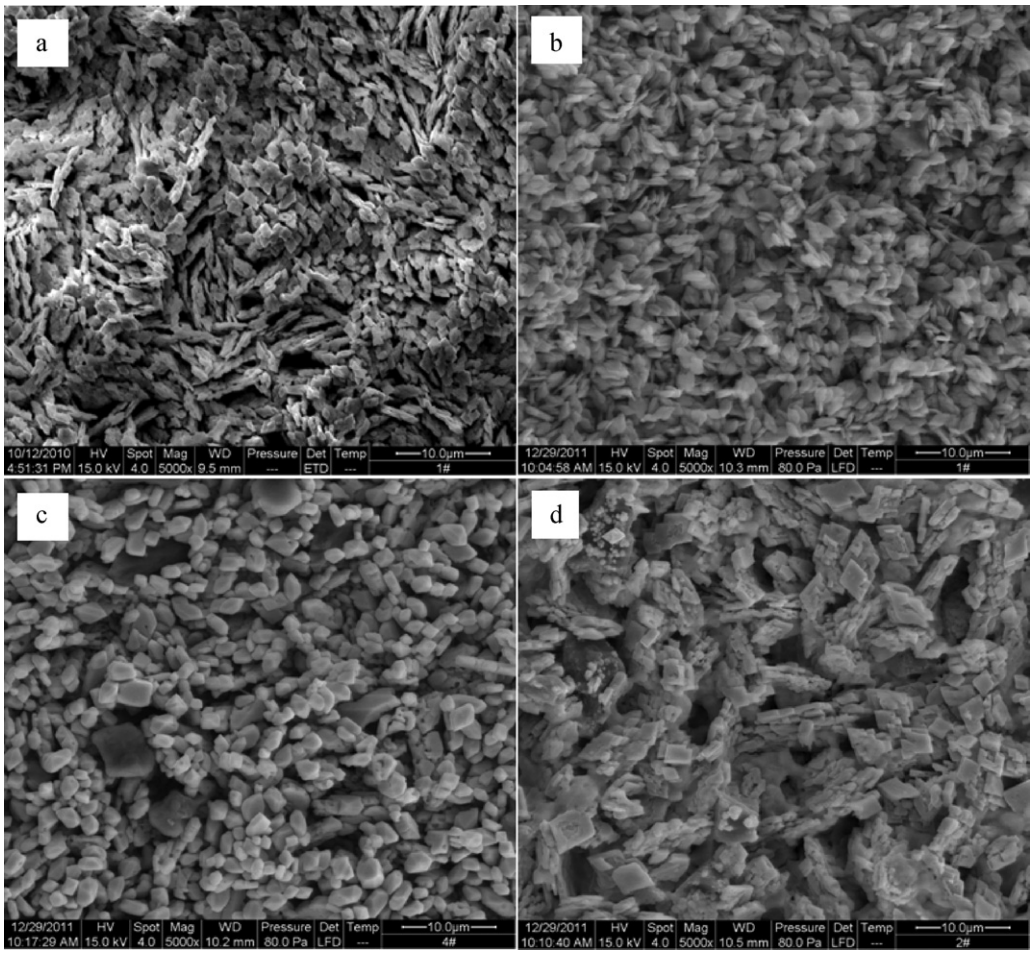

Fig. 3. SEM images of corrosion scales after cyclic voltammetries for 100 cycles on four electrodes in 4.5 mol L^{-1} H_2SO_4 solution. (a) Pb0.035%Ca1.2%Sn alloy, (b) Pb0.035%Ca1.2%Sn0.023%Yb alloy, (c) Pb0.035%Ca1.2%Sn0.048%Yb alloy and (d) Pb0.035%Ca1.2%Sn0.086%Yb alloy. $T = 25 \pm 0.5$ °C.

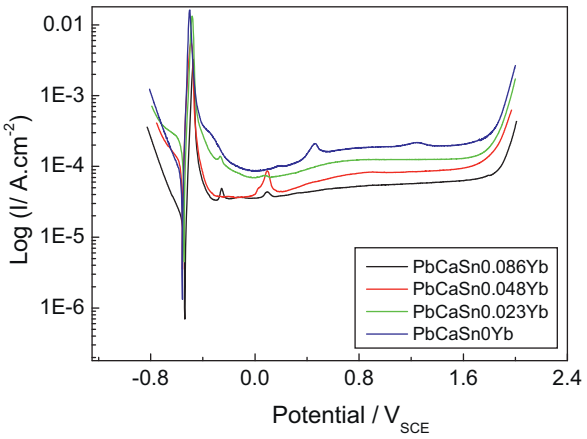

Fig. 4. The potentiodynamic curves of Pb0.035%Ca1.2%Sn, Pb0.035%Ca1.2%Sn0.023%Yb, Pb0.035%Ca1.2%Sn0.048%Yb, Pb0.035%Ca1.2%Sn0.086%Yb electrodes in 4.5 mol L^{-1} H_2SO_4 solution. $T = 25 \pm 0.5$ °C.

state is related to the formation of the passive film. The passive region in the steady passive state for Pb0.035%Ca1.2%Sn alloy electrode originates from −0.344 V to 1.67 V, while for other electrodes the passive regions are between −0.272 V and 1.783 V (Pb0.035%Ca1.2%Sn0.023%Yb alloy), between −0.088 V and 1.727 V (Pb0.035%Ca1.2%Sn0.048%Yb alloy) and between 0.015 V and 1.67 V (Pb0.035%Ca1.2%Sn0.086%Yb alloy), respectively. The corresponded steady passive current densities I_{ss} are 5.091E−5 A cm^{-2}, 7.903E−5 A cm^{-2}, 1.187E−4 A cm^{-2} and 1.843E−4 A cm^{-2}, respectively. Apparently, the steady passive region of PbCaSnYb alloy increases and the steady passive current density decreases with the increment of Yb content, it indicates that the protective effect of the passive film on PbCaSnYb alloy increases by increasing Yb content, this result is in agreement with the cyclic voltammetries.

3.3. Electrochemical impedance spectra (EIS) of the corrosion scale

3.3.1. EIS of the anodic film on PbCaSnYb at 1.28 V

The impedance spectra of anodic films on Pb0.035%Ca1.2%Sn, Pb0.035%Ca1.2%Sn0.023%Yb, Pb0.035%Ca1.2%Sn0.048%Yb and Pb0.035%Ca1.2%Sn0.086%Yb electrodes at 1.28 V for 12 h in 4.5 mol L^{-1} solution at 25 °C are depicted in Fig. 5, in which 1.28 V is chosen for the growth of the anodic film because this potential is in the growth potential region of PbO. Fig. 5a shows that the Nyquist plots display the similar feature, i.e., the Nyquist plots are consisted of two capacitive arcs at high and low frequencies, respectively. The semicircle of the Nyquist plot decreases with the increment of Yb content, the Bode plot (shown in Fig. 5b) shows that two different frequency regions appear, clearly pointed to the response of two different frequency-dependent processes with corresponding time constant, one constant time which appeared in the frequency region lower than 1 Hz originates from the space charge in the film/metal interface and the other appearing in the frequency region higher than 1 Hz may originated from the film/solution interface. As the anodic film on lead electrode at 1.28 V appears the structure of Pb/PbO/$PbSO_4$/electrolyte [15], therefore, the equivalent electron circuit shown in Fig. 6 is employed to fit the EIS, the equivalent electron circuit comprises the constant phase element (CPE), the impedance and admittance of CPE can be obtained with the following relationship [16,17]:

$$Z_{CPE} = [Y_0(j\omega)^n]^{-1} \quad (1)$$

$$Y_{CPE} = Y_0(j\omega)^n \quad (2)$$

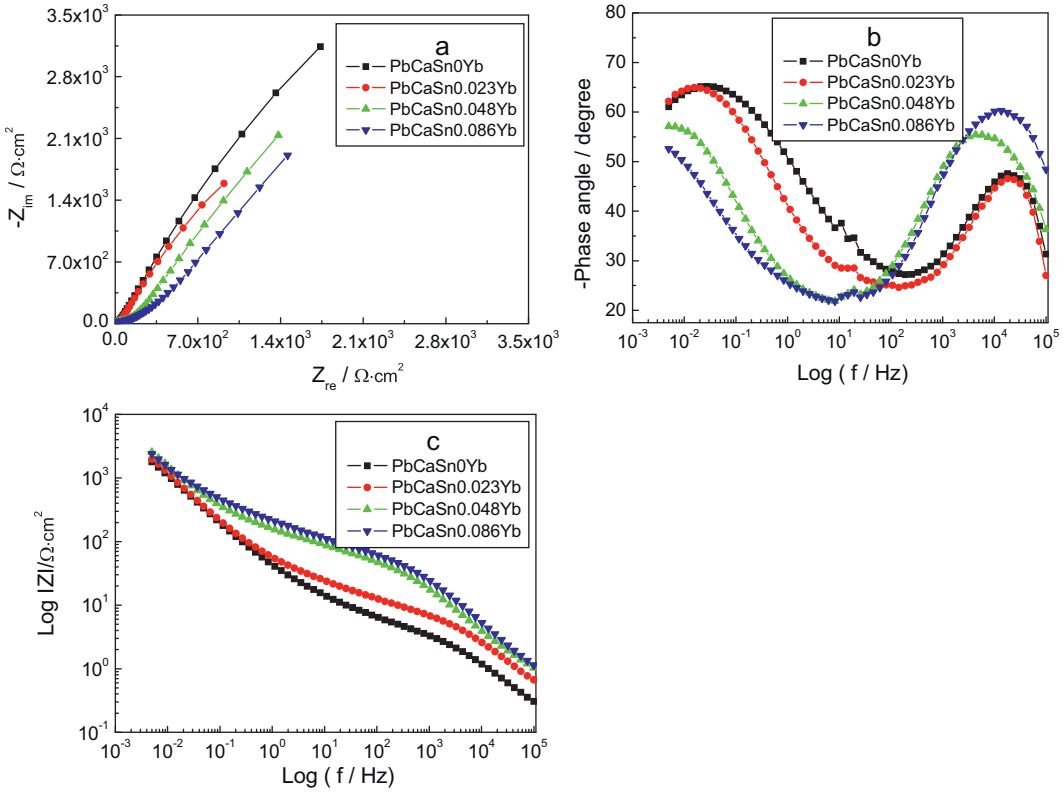

Fig. 5. The impedance spectra of the anodic films formed on four electrodes at 1.28 V for 12 h in 4.5 mol L^{-1} H_2SO_4 solution at 25 °C. (a) Nyquist plot; (b) corresponding Bode phase angle and (c) Bode impedance magnitude plots.

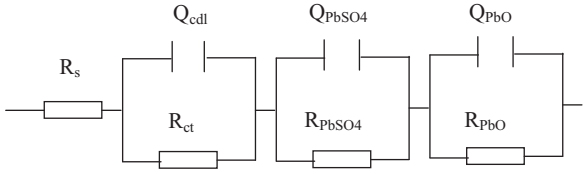

Fig. 6. The equivalent electron circuit used to fit the impedance spectra shown in Fig. 5, in which R_s is the solution resistance, Q_{cdl} and R_{cdl} represent the capacitance and resistance of the double layer, Q_{PbSO_4} and R_{PbSO_4} are related to the capacitance and resistance of $PbSO_4$ layer, Q_{PbO} and R_{PbO} are corresponding to the capacitance and resistance of PbO layer, respectively.

where j is the imaginary number, ω is the frequency of alternative current, exponent n is defined as the CPE power, which is adjusted between 0 and 1. For $n = 1$, the CPE describes an ideal capacitor with Y_0 equal to the capacitance C. For $n = 0$, the CPE is an ideal resistor. When $n = 0.5$, the CPE represents a Warburg impedance with diffusion character. While when $0.5 < n < 1$, CPE is the combination of properties related to both the surface and the electroactive species, and exponent n is the slope of the impedance–frequency Bode plot [18]. CPE has the properties of a capacitance when $0.5 < n < 1$, the CPE describes a frequency dispersion of time constants due to local inhomogeneous, porosity and roughness of the electrode surface.

The impedance data is checked for compliance with linear system theory by Kramers–Kronig transformation (shown in Fig. 7), it can be seen that the K–K transforms fit the experimental data well over the entire frequency range, it implies that the equivalent electron circuit can fit the EIS well.

The fitted results of the impedance spectra are listed in Table 2, it can be noticed that the resistances of $PbSO_4$ film (R_{PbSO_4}), PbO film (R_{PbO}) and the transfer resistance (R_{ct}) decrease, the values of Y corresponding to the capacitances of the double layer (Q_{cdl}), $PbSO_4$ film (Q_{PbSO_4}) and PbO film (Q_{PbO}) increase with the increment of Yb content. The value of the capacitances of the double layer, $PbSO_4$ film and PbO film can be acquired by calculating the effective capacitances from the corresponded CPE [19] as following:

$$C = Y_0^{1/n}(R_s^{-1} + R_{ct}^{-1})^{(n-1)/n} \quad (3)$$

In the above equation, R_s and R_{ct} are the solution resistance and the transfer resistance, respectively.

According to Eq. (3), the capacitances of $PbSO_4$ films within the anodic films on Pb0.035%Ca1.2%Sn, Pb0.035%Ca1.2%Sn0.023%Yb, Pb0.035%Ca1.2%Sn0.048%Yb and Pb0.035%Ca1.2%Sn0.086%Yb electrodes are 3.223E−7 F cm^{-2}, 1.292E−4 F cm^{-2}, 3.182E−4 F cm^{-2} and 1.827E−3 F cm^{-2}, respectively. The corresponded capacitances of the PbO films in case of four electrodes are 6.066E−5 F cm^{-2}, 4.317E−4 F cm^{-2}, 9.813E−4 F cm^{-2} and 1.449E−3 F cm^{-2}, respectively. Evidently, the capacitances of $PbSO_4$ and PbO films sharply increase with the increment of Yb content. The increment of capacitance and decrement of resistance indicating a rough and inhomogeneous character of the anodic film, then it can be concluded that the micro-channel within $PbSO_4$ and PbO film increases with increasing Yb content, and the ions easily passed through the anodic film, finally the conductivity of the anodic film enhances.

The influence of Yb content on the electrochemical property of the anodic film on PbCaSn alloy in 4.5 mol L^{-1} H_2SO_4 solution can be illustrated by the SEM images (Fig. 8) of anodic films on four electrodes at 1.28 V_{SCE} for 12 h in 4.5 mol L^{-1} solution, it can be seen that the anodic film on Pb0.035%Ca1.2%Sn alloy electrode is consisted of fine and compact crystals, the crystal grows and the anodic film becomes porous with the addition of Yb. As Yb content continues to increase, the crystal grows faster, and the porosity significantly increases. The increased porosity can make the ions (including H^+, H_2O and SO_4^{2-}) easily pass through the anodic film on PbCaSnYb alloy, and then the conductivity of the anodic film increases.

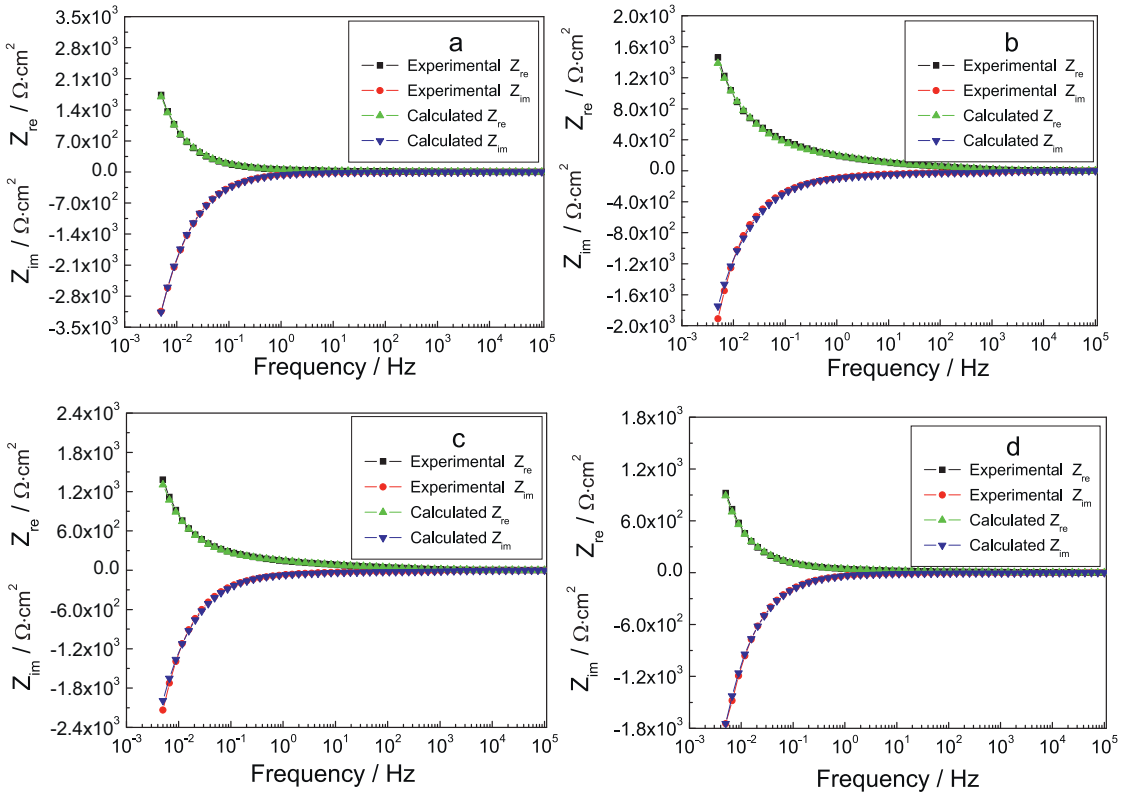

Fig. 7. Kramers–Kronig transforms of the real and imaginary components of the electrochemical impedance of the anodic films on four electrodes at 1.28 V (SCE) for 12 h in 4.5 mol L^{-1} H_2SO_4 solution. $T = 25 \pm 1$ °C.

Table 2
The fitted results of the impedance spectra.

Elements	PbCaSn–0Yb	PbCaSn–0.023Yb	PbCaSn–0.048Yb	PbCaSn–0.086Yb
R_s (Ω cm^2)	0.3047	0.3127	0.5013	0.3757
Y_{cdl} (Ω^{-1} S^n)	4.569E–5	1.164E–4	4.314E–3	5.073E–3
n_{cdl}	0.779	0.7679	0.723	0.525
R_{ct} (Ω cm^2)	50.5	46.88	43.19	30.58
Y_{PbSO_4} (Ω^{-1} S^n)	1.14E–4	1.521E–3	3.661E–3	7.588E–3
n_{PbSO_4}	0.606	0.7563	0.5911	0.8045
R_{PbSO_4} (Ω cm^2)	136.6	112.5	26.76	5.349
Y_{PbO} (Ω^{-1} S^n)	3.981E–3	4.034E–3	7.068E–3	8.425E–3
n_{PbO}	0.6161	0.7492	0.7559	0.7658
R_{PbO} (Ω cm^2)	5.688E4	3.26E4	2.535E4	1.99E4

3.3.2. *EIS of the corrosion scale on four electrodes after cyclic voltammetries for 100th*

For maintenance-free lead acid battery, a serious problem is the deep recycle behavior, the reason maybe related to the formation of the corrosion scale with the high resistance on grid surface. Generally, the PbO/$PbSO_4$·PbO corrosion system is recognized as the major component of the corrosion scale with high resistance [5,6], therefore, it is vital to decrease the resistance of the PbO/$PbSO_4$·PbO corrosion system for the novel grid alloy. In order to evaluate the deep recycle property of PbCaSnYb alloy, EIS of the corrosion scales after cyclic voltammetries for 1000th on four electrodes in 4.5 mol L^{-1} H_2SO_4 solution at 25 °C are measured, the results are shown in Fig. 9. Fig. 9a shows that the Nyquist plots are all consisted of two capacitance arcs, relating to the formation of the $PbSO_4$·PbO and PbO_2 corrosion scales (considering the potential region of CV experiment is within the growth potential regions of $PbSO_4$·PbO and PbO_2 systems [20]). The Bode plot shown in Fig. 9b can be divided into two sections below and above 1 Hz, in which the phase angle increases with the increment of Yb content in the region from 10^5 Hz to 1 Hz, indicating the increased film (PbO_2 film) resistance. While the phase angle decreases with the increment of Yb content in the region from 1 Hz to 0.001 Hz, implying the decrement of the film ($PbSO_4$·PbO film) resistance. The Bode impedance magnitude plot presents three straight line segments, indicating the corrosion process is dependent on three time constants. Therefore, an equivalent electron circuit shown in Fig. 10 is used to fit

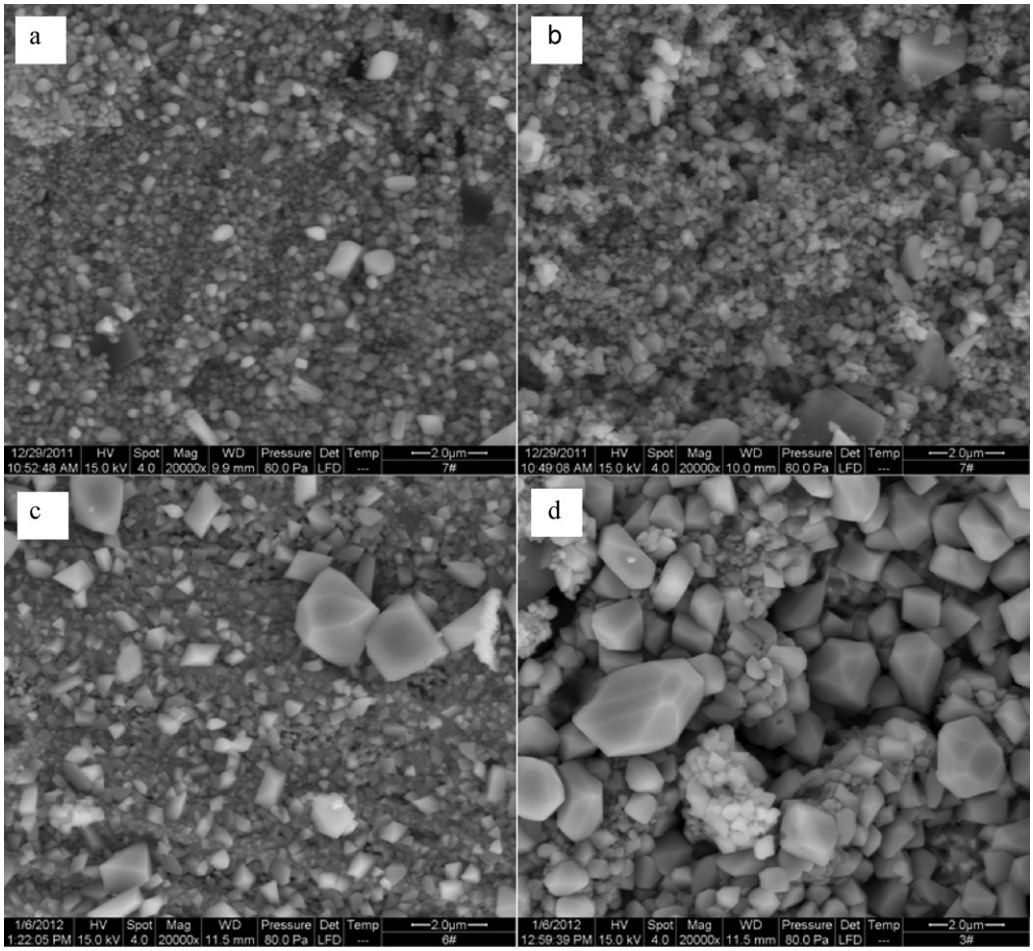

Fig. 8. SEM images of anodic films on four electrodes at 1.28 V_{SCE} for 12 h in 4.5 mol L^{-1} H_2SO_4 solution. (a) Pb0.035%Ca1.2%Sn alloy, (b) Pb0.035%Ca1.2%Sn0.023%Yb alloy, (c) Pb0.035%Ca1.2%Sn0.048%Yb alloy and (d) Pb0.035%Ca1.2%Sn0.086%Yb alloy. $T = 25 \pm 0.5$ °C.

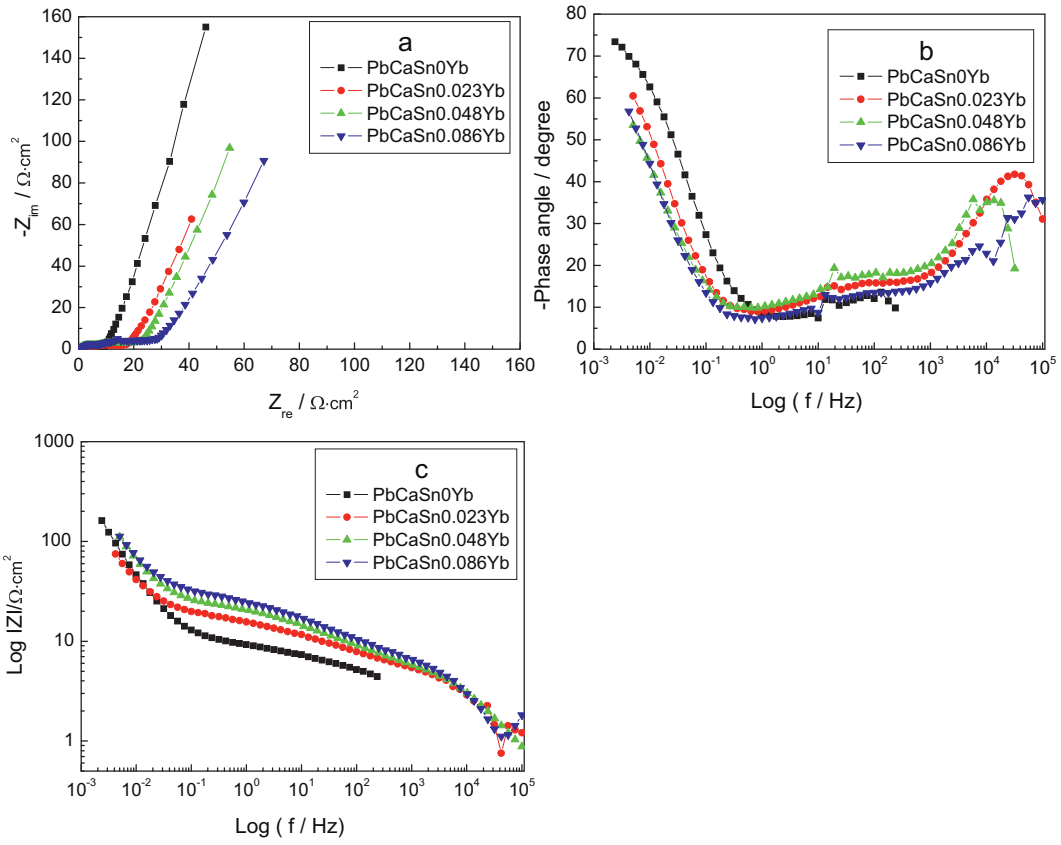

Fig. 9. The impedance spectra of corrosion scales after cyclic voltammetries for 1000th on four electrodes in 4.5 mol L^{-1} H_2SO_4 solution at 25 °C, (a) Nyquist plot; (b) corresponding Bode phase angle and (c) Bode impedance magnitude plots.

the impedance spectra. The total impedance can be calculated as following:

$$Z_{\text{total}} = R_s + \frac{1}{Y_{\text{cdl}}(j\omega)^n + (1/R_{\text{ct}})} + \frac{1}{Y_{\text{PbSO}_4\cdot\text{PbO}}(j\omega)^n + (1/R_{\text{PbSO}_4\cdot\text{PbO}})} + \frac{1}{Y_{\text{PbO}_2}(j\omega)^n + (1/R_{\text{PbO}_2})} \quad (4)$$

Using Eq. (4), the calculated results are shown in Table 3, it can be seen that all fitted variances are below 10^{-3}, implying the good simulation of the impedance using the equivalent electron circuit. The resistances of PbO_2 films slightly increase and the capacitances of PbO_2 films decrease with the increment of Yb content, this manifests that the addition of Yb into PbCaSn alloy may inhibit the growth of PbO_2 in the corrosion scale after recycle. While the resistance of $PbSO_4$·PbO film rapidly decreases and the corresponding capacitance increases with the increment of Yb content, the decrement of the resistance of $PbSO_4$·PbO film can be vitally important to improve the deep recycle property of the lead acid battery. The increased capacitance of $PbSO_4$·PbO film may be related to the increased porosity of the corrosion scale, and the ions can easily pass through the $PbSO_4$·PbO film, then the charge–discharge process of the lead acid battery is easily occurred.

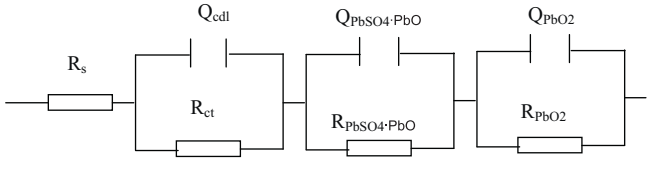

Fig. 10. The equivalent electron circuit used to fit the impedance spectra shown in Fig. 9, in which R_s is the solution resistance, Q_{cdl} and R_{cdl} represent the capacitance and resistance of the double layer, $Q_{\text{PbSO}_4\cdot\text{PbO}}$ and $R_{\text{PbSO}_4\cdot\text{PbO}}$ are related to the capacitance and resistance of $PbSO_4$·PbO layer, Q_{PbO_2} and R_{PbO_2} are corresponding to the capacitance and resistance of PbO_2 layer, respectively.

3.4. Linear sweep voltammetry (LSV)

Fig. 11 shows the voltammograms of anodic films formed on four electrode at 1.28 V and 25 °C for 12 h in 4.5 mol L^{-1} H_2SO_4 solution. It can be seen that two reduction peaks can be observed in Fig. 11, in which peak a represents the reduction of Pb(II) (like

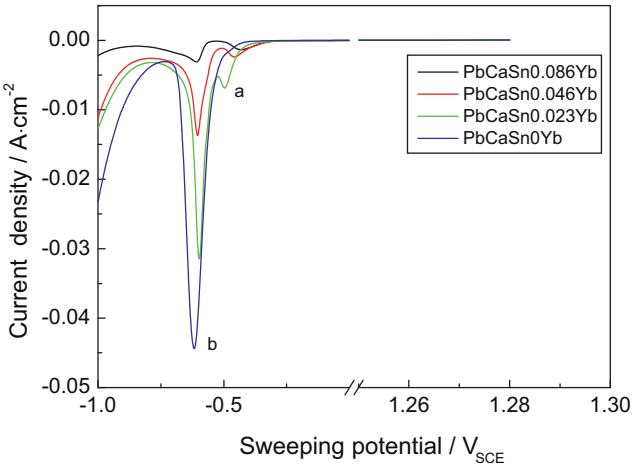

Fig. 11. The linear sweeping voltammetries of anodic films formed on four electrodes at 1.28 V for 12 h in 4.5 mol L^{-1} H_2SO_4 solution. $T = 25 \pm 0.5$ °C.

Table 3
The fitted results of the impedance spectra shown in Fig. 10.

Elements	PbCaSn–0Yb	PbCaSn–0.023Yb	PbCaSn–0.048Yb	PbCaSn–0.086Yb
R_s ($\Omega\,cm^2$)	0.358	0.3188	0.4097	0.45
Y_{cdl} ($\Omega^{-1}\,S^n$)	8.322E−5	1.107E−5	1.61E−4	1.815E−4
n_{cdl}	1	0.7007	1	1
R_{ct} ($\Omega\,cm^2$)	3.56	3.127	2.317	1.635
$Y_{PbSO_4\cdot PbO}$ ($\Omega^{-1}\,S^n$)	0.2602	0.3687	0.2292	0.1645
$n_{PbSO_4\cdot PbO}$	0.8725	0.8735	0.903	0.7906
$R_{PbSO_4\cdot PbO}$ ($\Omega\,cm^2$)	2791	813	650.8	513.2
Y_{PbO_2} ($\Omega^{-1}\,S^n$)	2.346E−2	1.607E−2	9.687E−3	5.679E−3
n_{PbO_2}	0.9398	0.6311	0.8732	0.94
R_{PbO_2} ($\Omega\,cm^2$)	8.107	18.27	24.91	25.18
$\sum\chi^2$	2.52E−3	1.164E−3	2.582E−3	8.107E−3

PbO, PbO·$PbSO_4$ and 3PbO·$PbSO_4$) to Pb, and peak b is caused by the reduction of $PbSO_4$ to Pb [13]. The two peak currents evidently decrease with the increment of Yb content, it demonstrates that Yb may inhibit the growth of Pb(II) compounds in the anodic film formed on PbCaSn alloy, this result is in agreement with the EIS result of the anodic film.

3.5. Mott–Schottky analysis

The semi-conductive property of the passive film on metal or alloy is often studied by Mott–Schottky analysis based on the measurement of the electrode capacitance as a function of the applied potential, the reciprocal of the square of the capacitance (C) and the applied potential (E) obey the linear relationship under the depletion condition. For an n-type semiconductor [21–26]:

$$C^{-2} = C_{SC}^{-2} + C_H^{-2} = \frac{2}{\varepsilon\varepsilon_0 e N_D}\left(E - E_{FB} - \frac{KT}{e}\right) + C_H^{-2} \quad (5)$$

where C_{SC} is the space charge capacitance of the passive film, C_H is the Helmholtz layer capacitance, which is assumed to have a constant value of 20 $\mu F\,cm^{-2}$ [27]. Considering the space charge capacitance C_{SC} is much less than that of the Helmholtz capacitance C_H, and thus the electrode capacitance C is equal to C_{SC}, then the Mott–Schottky equation can be written as:

$$C^{-2} = C_{SC}^{-2} = \frac{2}{\varepsilon\varepsilon_0 e N_D}(E - E_{FB} - \frac{KT}{e}) \quad (6)$$

in which e is the electron charge (1.602×10^{-19} C), N_D is the donor density, ε is the dielectric constant of the passive film, ε_0 is the vacuum permittivity ($8.854 \times 10^{-14}\,F\,cm^{-1}$), K is the Boltzmann constant ($1.38 \times 10^{-23}\,J\,K^{-1}$), T is the absolute temperature and E_{FB} is the flat band potential. The term KT/e can be neglected because it is only about 25 mV at room temperature. N_D can be determined from the slope of the experimental C^{-2} versus E plot, and E_{FB} can be obtained from the extrapolation of the linear portion to $C^{-2} = 0$.

Fig. 12 shows the Mott–Schottky plots of the anodic films on four electrodes at 1.28 V for 12 h in 4.5 mol L^{-1} solution at 25 °C, it can be seen that the slope of the Mott–Schottky plot appears positive indicating an n-type semi-conductive character of the anodic film on PbCaSnYb alloy. For the anodic film on lead alloy at 1.28 V in sulfuric acid solution, the major components are Pb(II) (PbO and $PbSO_4$), in which PbO is an oxide conductor with interstitial oxygen (PbO_{1+x}) based on the crystallography, therefore, PbO has p-type semi-conductive character. However, the positive slopes of M–S plots meaning the n-type semi-conductive performance of the anodic film, herewith, there existing the oxides with n-type semi-conductive within the anodic film. Comparing with the EIS result of the increased conductivity of the anodic film with Yb, it can be concluded that PbO_2 may exist in the anodic film, and the content of PbO_2 may increase in the anodic film with increasing Yb content, therefore, the anodic film can be deemed as the mixture of PbO and PbO_2 (PbO_2 has n-type semi-conductive character), only in this way, the n-type semi-conductive behavior of the anodic film on four electrodes can be explained, this result is also in accordance with Bojinov et al. [28].

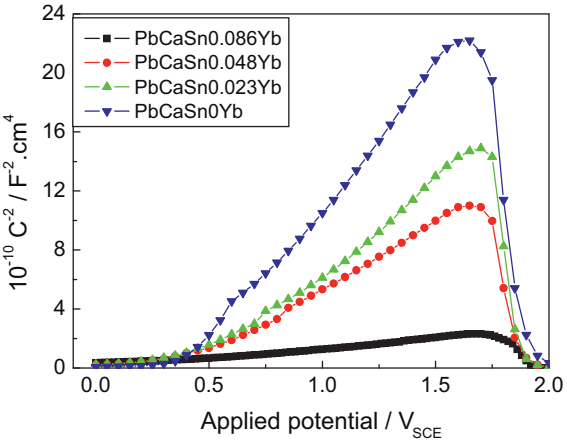

Fig. 12. The Mott–Schottky plots of the anodic films on four electrodes at 1.28 V for 12 h in 4.5 mol L^{-1} H_2SO_4 solution at 25 °C.

The slopes of the Mott–Schottky plots sharply decrease with the increment of Yb content, it implies that the defect densities within the anodic film increase with Yb content based on Eq. (6). The defect existed in the anodic film can act as the charge carrier, and then the increased defect densities indicate the improved conductivity of the anodic film, this result is in accordance with the results of EIS and LSV.

4. Conclusion

The addition of Yb into PbCaSn alloy can affect its electrochemical behaviors in 4.5 mol L^{-1} H_2SO_4 solution. Yb can improve the corrosion resistance of PbCaSn alloy in H_2SO_4 solution by decreasing the reduction of PbO_2. The addition of Yb can significantly decrease the resistance of Pb(II) film in the anodic film, it is vitally important to promote the deep recycle property of the lead acid battery. The anodic film on PbCaSnYb alloy appears n-type semi-conductive character, the defect density within the anodic film increases with the increment of Yb content.

Acknowledgment

This work is supported by the National Natural Science Foundation of China (Grant No. 51021064).

References

[1] B. Manahov, D. Pavlov, J. Electrochem. Soc. 141 (1994) 2316–2326.
[2] D. Pavlov, J. Power Sources 46 (1993) 171–190.
[3] D. Pavlov, B. Monakhov, M. Maja, J. Electrochem. Soc. 136 (1989) 27–33.
[4] J.L. Caillerie, L. Albert, J. Power Sources 67 (1997) 279–281.
[5] C. Brissaud, G. Reumont, J.P. Smaha, J. Foct, J. Power Sources 64 (1997) 117–122.
[6] A.F. Hollenkamp, J. Power Sources 59 (1996) 87–98.
[7] H.K. Giess, J. Electrochem. Soc. 131 (1984) C284.
[8] N. Bui, P. Mattesco, P. Simon, J. Steinmetz, E. Rocca, J. Power Sources 67 (1997) 61–67.
[9] H.-T. Liu, J. Yang, H.-H. Liang, W.-F. Zhou, J. Fudan Univ. (Nat. Sci.) 38 (1999) 623–626.
[10] Y.-B. Zhou, C.-X. Yang, W.-F. Zhou, H.-T. Liu, J. Alloys Compd. 365 (2004) 108–111.
[11] M. Alexandre, G. Bourguignon, J.M. Fiorani, J. Ghanbaja, J. Steinmetz, Mater. Sci. Eng. A 358 (2003) 233–242.
[12] D.-G. Li, G.-S. Zhou, G.-F. Lin, M.-S. Zheng, J. Rare Earths 23 (2005) 353–358.
[13] J. Han, C. Pu, W.F. Zhou, J. Electroanal. Chem. 368 (1994) 43–46.
[14] H.T. Liu, J. Yang, H.H. Liang, J.H. Zhang, W.F. Zhou, J. Power Sources 93 (2001) 230–233.
[15] K.R. Bullock, M.A. Butler, J. Electrochem. Soc. 133 (1986) 1085–1090.
[16] J. Hubrecht, M. Embrechts, W. Bogaerts, Electrochim. Acta 38 (1993) 1867–1875.
[17] M. Cai, S.M. Park, J. Electrochem. Soc. 143 (1996) 3895–3902.
[18] L. Hamadou, A. Kadri, N. Benbrahim, Appl. Surf. Sci. 252 (2005) 1510–1519.
[19] H.P. Scott, D.M. Thomas, J. Electrochem. Soc. 155 (2008) C381–C386.
[20] Z. Takehara, K. Kanamura, K. Kawanam, J. Electrochem. Soc. 137 (1990) 800–804.
[21] R. De Gryse, W.P. Gomes, F. Cardon, J. Vennik, J. Electrochem. Soc. 122 (1975) 711–712.
[22] N.E. Hakiki, M. Da Cunha Belo, A.M.P. Simões, M.G.S. Ferreira, J. Electrochem. Soc. 145 (1998) 3821–3829.
[23] S.R. Morrison, Electrochemistry at Semiconductor and Oxidized Electrodes, Plenum Press, New York, 1980.
[24] K. Darowicki, S. Krakowiak, P. Slepski, Electrochim. Acta 51 (2006) 2204–2208.
[25] H.O. Finklea, J. Electrochem. Soc. 129 (1982) 2003–2008.
[26] N.E. Hakiki, M. Da Cunha Belo, J. Electrochem. Soc. 143 (1996) 3088–3094.
[27] F. Di Quarto, A. Di Paola, C. Sunseri, J. Electrochem. Soc. 127 (1980) 1016–1021.
[28] M. Bojinov, K. Solmi, G. Sundholm, Electrochim. Acta 39 (1994) 719–726.